J Infrared Milli Terahz Waves (2010) 31:169–180
DOI 10.1007/s10762-009-9577-4

The Impact of Slow-Wave Modes on the Radiation Performance of a Corrugated Horn Antenna

Philipp Fürholz · Axel Murk

Received: 20 November 2008 / Accepted: 9 September 2009 /
Published online: 16 September 2009

Abstract Corrugated horn antennas offer many advantages compared with other waveguide radiators. A major disadvantage which is inherent with the design of a corrugated horn is the fact that slow-wave modes may exist within the horn antenna. In this paper far-field measurements of a W-band horn antenna are presented. The experimental data is compared with simulated data to confirm the presence of slow-wave modes. The analysis is completed by determining the waist, the gaussicity and the phase center location of both the experimental and model data. Finally a redesign approach is proposed which suppresses the slow-wave modes and therefore increases the usable bandwidth of the horn antenna.

Keywords Horn antenna · Slow-wave modes · Antenna pattern · Gaussian beam analysis

1 Introduction

Corrugated horn antennas are nowadays a standard for a radiator at cm to submm-wavelength because of their bandwidth, high pattern symmetry, low sidelobes and low crosspolar level. The basic mathematical foundation was given by [1], which proposed the excitation of a TM_{11} mode to obtain a circular symmetric beam pattern with low crosspolar signal. The so-called Potter Horn, however, can be operated only in a narrow band. In [2] it is shown that a similar pattern can be obtained using a geometry with a dielectric layer placed on the metallic walls. This allows the propagation of a hybrid mode. Practically this surface impedance condition is obtained by machining small corrugations into the metallic walls. Design and optimization of corrugated horns is nowadays an important research topic for

P. Fürholz (✉) · A. Murk
Institute of Applied Physics, Berne, Switzerland
e-mail: fuerholz@gmx.ch

many research groups. For instance the length of a corrugated horn antenna has been successfully reduced while maintaining the radiation behavior. Also other propagation phenomena such as left-handed wave propagation inside a corrugated waveguide are studied. This paper deals with the experimental characterization of the radiation patterns of a W-band aperture-limited corrugated horn antenna operating in a frequency band ranging from 75 to 110 GHz. A previous study, which aimed mainly at an experimental quality assessment [3] of the horn antenna, revealed the presence of slow-wave modes. An independent study [4] predicts the presence of slow-wave modes inside corrugated horn antennas. The paper is organized as follows. In part one two analysis techniques are reviewed. Part two describes the measurement setup and the experimental results along with the gaussian beam analysis. In the third part possible optimization of the horn geometry is shown which reduces the presence of slow-wave modes.

2 Modeling approaches of the horn antenna

Beam patterns of corrugated horn antennas can be predicted using electromagnetic simulation methods such as the method of moments [5] or finite elements [6]. Taking advantage of the horn geometry also the mode-matching technique can be used. All of the listed methods need very few physical approximations, therefore they are able to model a corrugated horn antenna accurately. However, due to their complexity, they lack of physical insight. For this reason in this paper a rather simplistic approach has been chosen beside the mode-matching technique to model the horn antenna. The surface impedance approach [7] simply consists in the calculation of the propagation constants of the hybrid modes inside the horn. Although very approximative this approach gives physical understanding of the propagation processes inside the horn antenna.

2.1 Surface impedance approach

Assuming corrugations enough thin and closely packed to each other ($\ll \lambda$) the corrugated layer can be seen as a dielectric with a certain surface impedance. For this geometry analytical solutions for Maxwell's equations can be found. For the solution of Maxwell's equation for a corrugated waveguide geometry we distinguish between the inner waveguide with radius r_1 and the corrugated part. The total radius of the waveguide is denoted r_0, a denotes the aperture radius and ξ_{nm} the n'th zero of the bessel function of order m. In cylindrical coordinates the solution for the electric and magnetic field in the inner part reads

$$E_z(r, \phi, z) = \sum_{mn} A_{mn} J_m((\xi_{nm}/a)r) \exp(ik_z z) \cos(m\phi) \tag{1}$$

$$H_z(r, \phi, z) = \sum_{mn} B_{mn} J_m((\xi_{nm}/a)r) \exp(ik_z z) \sin(m\phi) \tag{2}$$

with A_{mn} and B_{mn} being normalization constants and k_z being the axial propagation constant. Within the slots the field solution reads

$$E_z = CS_m(k_0 r_1, k_0 r_0)\cos\left(\frac{2P\pi z}{b}\right) - iCS'_m(k_0 r_1, k_0 r_0)\sin\left((2P-1)\frac{\pi}{b}z\right)\exp(im\phi) \tag{3}$$

$$H_z = -iDS_m(k_0 r_1, k_0 r_0)\sin\left(\frac{2P\pi z}{b}\right) + DR'_m(k_0 r_1, k_0 r_0)\cos\left((2P-1)\frac{\pi}{b}z\right)\exp(im\phi) \tag{4}$$

with b denoting the slot width, P an integer mode number, C,D being normalization constants and k_0 denoting the free space propagation constant. R_m and S_m denote cylindrical functions defined as

$$R_m(x, y) = J_m(x)Y'_m(y) - J'_m(y)Y_m(x) \tag{5}$$

$$S_m(x, y) = J_m(x)Y_m(y) - J_m(y)Y_m(x) \tag{6}$$

with J and Y being the bessel functions of the first and second kind. The boundary conditions require the surface admittance H_ϕ/E_z to be constant at $r = r_1$. We first reexpress H_z using the normalized impedance Γ.

$$H_z = -A_{mn} i\sqrt{\epsilon_0/\mu_0}J_m(k_r r)(mk_z + \Gamma F_m(k_r r))\exp(im\phi) \tag{7}$$

with F_m being

$$F_m(x) = \frac{xJ'_m(x)}{J_m(x)} \tag{8}$$

and k_r denoting the radial propagation constant. The slot width is assumed to be sufficiently small so that only a TM standing wave can be present in the slots. Therefore E is zero at r_1. Equation 6 yields

$$mk_z - \Gamma F_m(k_r r_1) = 0 \tag{9}$$

The surface admittance boundary condition yields

$$F_m(k_r r_1) - \frac{m^2(k_z/k_0)^2}{F_m(k_r r_1)} = \left(\frac{k_r r_1}{k_0 r_1}\right)^2 S_m(k_0 r_1, k_0 r_0) \tag{10}$$

Equation 10 relates the free-space propagation constant k_0 to the propagation in z-direction k_z for a given waveguide geometry. Therefore with this equation the dispersion curves for the hybrid modes can be computed. Contrary to regular waveguide modes also imaginary solutions are allowed for k_r, modes with $k_z > k_0$ are called slow-wave modes. Since the operation bandwidth of the horn antenna to be examined is quite large we computed the dispersion diagram for several positions along the horn geometry. Ideally at the throat of the horn the dispersion curve should be equal to a TE_{11} mode. At the end of mode-converter section we expect a single dispersion curve of a hybrid HE_{11} mode. As the inner radius increases higher order HE_{1n} modes can propagate.

2.2 Mode-matching

For straight perfect electric conductor (PEC) bounded waveguide structures the 2-port scattering coefficient, the aperture fields at both ends of the waveguide and quantities derived from the aperture fields such as the far-field pattern can be computed using the so-called mode-matching (MM) technique [8]. The idea behind MM is to discretise the waveguide into pieces of constant cross-section. At the junction between two subsections the boundary conditions for the electric and magnetic fields are enforced. For a subsection the electric and magnetic field can be expressed as a superposition of modes propagating in both directions

$$\vec{E} = \sum_m \sqrt{Z_m} \left(A_m^+ + A_m^-\right) \vec{e_m} \tag{11}$$

with A_m^+ denoting the the m'th mode propagating in one direction and A_m^- denoting the m'th mode propagating in the opposite direction. For the magnetic field the superposition reads

$$\vec{H} = \sum_m \frac{1}{\sqrt{Z_m}} \left(A_m^+ - A_m^-\right) \vec{h_m} \tag{12}$$

At a waveguide junction the electric and magnetic fields must be continuous over the common surface. Over the PEC surface of the junction the tangential electric field must vanish. Using Eqs. 11 and 12 for the electric and magnetic field this yields

$$\sum_m \frac{1}{\sqrt{Z_m}} \left(A^+ - A_m^-\right) \vec{h_m} = \sum_m \frac{1}{\sqrt{Z_m}} \left(B_m^+ - B_m^-\right) \vec{h_m} \text{ on } \Omega_1 \tag{13}$$

$$\sum_m \sqrt{Z_m} \left(A_m^+ + A_m^-\right) \vec{e_m} = \sum_m \sqrt{Z_m} \left(B_m^+ + B_m^-\right) \vec{e_m} \text{ on } \Omega_1 \tag{14}$$

$$\sum_m = \sqrt{Z_m} \left(A_m^+ + A_m^-\right) \vec{e_m} = 0 \text{ on } \Omega_2 \tag{15}$$

with A being the mode coefficients for the larger waveguide and B being the coefficients for the smaller waveguide. Ω_1 denotes the common surface and Ω_2 the PEC surface. These equations now have to be turned into an expression which relates the mode coefficients for the incoming modes to the outgoing modes. This is achieved by multiplying Eqs. 13–15 with a testing function and integration over the cross-section of the waveguide. This then yields

$$\begin{pmatrix} A^- \\ B^+ \end{pmatrix} = \begin{pmatrix} S_{11} & S_{12} \\ S_{21} & S_{22} \end{pmatrix} \begin{pmatrix} A^+ \\ B^- \end{pmatrix} \tag{16}$$

with

$$\begin{aligned} S_{11} &= (T\hat{Z}\hat{Z}^* T^t Z^{-1*} + Z)^{-1} (T\hat{Z}\hat{Z}^* T^t Z^{-1*} - Z) \\ S_{12} &= 2(T\hat{Z}\hat{Z}^* T^t Z^{-1*} + Z)^{-1} T\hat{Z} \\ S_{21} &= (\hat{Z^{-1*}} + T^t Z^{-1*} Z^{-1} T\hat{Z})^{-1} (\hat{Z^{-1*}} - T^t Z^{-1*} Z^{-1} T\hat{Z}) \\ S_{22} &= 2T^t Z^{-1*} (\hat{Z^{-1*}} + T^t Z^{-1*} Z^{-1} T\hat{Z})^{-1} \end{aligned} \tag{17}$$

with Z and $\hat{Z}$ being the impedance matrix for the modes in the two waveguide pieces and T the coupling integrals matrix. For a straight waveguide piece with constant cross-section and length d the scattering matrice contains the phase delay expression $\exp(ik_z d)$

$$\begin{pmatrix} A^- \\ B^+ \end{pmatrix} = \begin{pmatrix} 0 & P \\ P & 0 \end{pmatrix} \begin{pmatrix} A^+ \\ B^- \end{pmatrix} \tag{18}$$

where P denotes the submatrices containing the phase delay expressions. In order to compute propagation through an entire waveguide structure the scattering matrices for several junctions and straight pieces have to be combined into a single one. For two successive scattering matrices the total scattering matrice can be computed using

$$\begin{aligned} S^c_{11} &= \left[S^a_{11} + \left(1 - S^b_{11} S^a_{22}\right)^{-1} S^b_{11} S^a_{21} \right] \\ S^c_{12} &= S^a_{12} P \left(1 - S^b_{11} S^a_{22}\right)^{-1} S^b_{12} \\ S^c_{21} &= S^b_{21} P \left(1 - S^a_{22} S^b_{11}\right)^{-1} S^a_{21} \\ S^c_{22} &= S^b_{21} \left(1 - S^a_{22} S^b_{11}\right)^{-1} S^a_{22} S^b_{12} + S^b_{22} \end{aligned} \tag{19}$$

3 Experimental setup and results

The experimental work done for this study consists in the measurement of the far-field pattern and the return loss of a W-Band corrugated horn for the entire frequency range of operation. The measurements were done using an ABmm vector network analyzer. The antenna under test (AUT) was mounted on a rotary table movable in azimuth and elevation direction. As a probe antenna a single-moded rectangular waveguide placed at ≈ 2 m from the AUT was used. The angular range is ± 60 degrees in elevation, the angular resolution for the measurement is 0.5°. The measurement environment in the laboratory was carefully covered with microwave absorbing material in order to prevent interference due to multi-path signals. The co-polar pattern has been measured at azimuth values of zero and ninety degrees, the cross-polar pattern at fortyfive degrees. As already stated the pattern have been measured over a wide frequency range which was close to one octave, namely ranging from 65 to 110 GHz.

The return loss was measured using a directional coupler attached to the feed of the horn antenna. The S_{11} measurements were calibrated using a standard W-band calibration kit consisting of a short, a matched load and an offset shim. The return loss measurements were done with the rectangular to circular waveguide transition attached to the horn, in the simulations this is not taken into account.

3.1 Results

The AUT has a opening angle of 4.95°, a total length of 9.4 cm and an aperture radius of 1 cm. Because of the small opening angle and electrically large aperture surface the AUT can be classified into the aperture-limited horn antenna. For an aperture-limited antenna the far-field beam alters its width with the frequency because the center of the best-fit gaussian is located more or less frequency independent at the

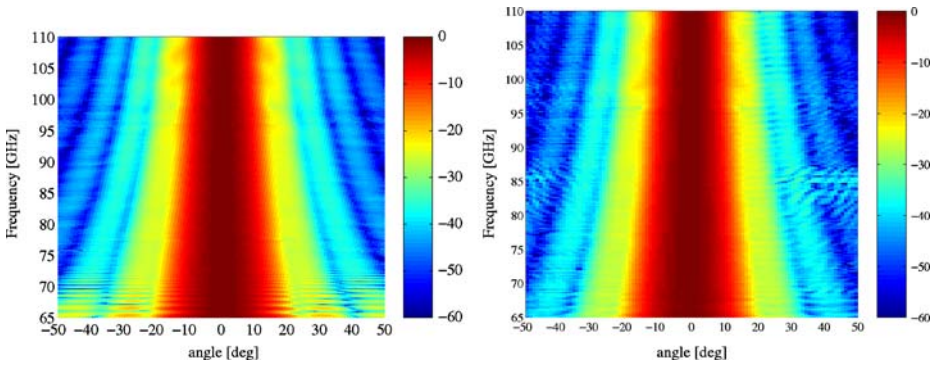

Fig. 1 Measured e-plane (*left*) and h-plane (*right*) copolar pattern over elevation and frequency.

aperture of the antenna. Thefore the relation best-fit gaussian beam size to free-space wavelength varies resulting in a narrower far-field pattern for high frequencies and a broader far-field pattern for lower frequencies.

This basic assumption is nicely verified in the measurement (Fig. 1). Both the e and h-plane pattern show a narrowing of the beam with increasing frequency. However in the lower band end we observe a rapid oscillation of the side-lobe level with frequency. Since these are also visible in the simulations based on mode-matching (Fig. 2), errors in the experimental setup or measurement technique can be excluded. This is where the slow-wave modes come into play. To understand the oscillation effects occurring in the lower end of the frequency band we computed the propagation constants of the hybrid modes for the entire frequency range and for several positions along the horn geometry. It shows that slow-wave modes occur along the entire horn for a certain frequency range. The upper limit for the axial propagation constant is

$$k_{z,max} = \frac{\pi}{d} \tag{20}$$

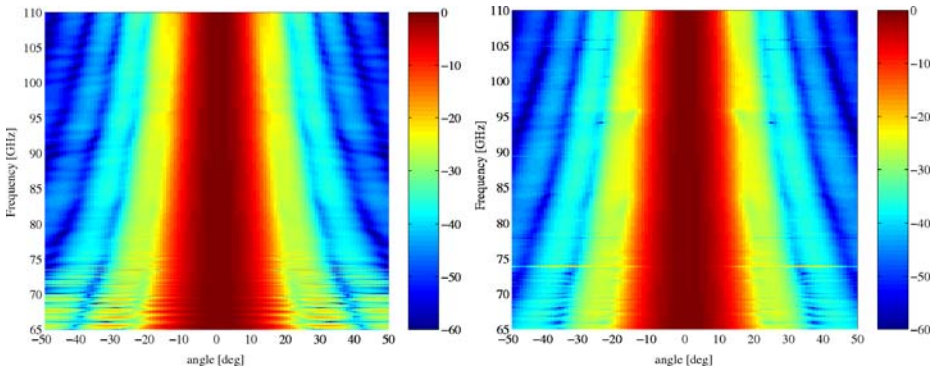

Fig. 2 Simulated e-plane (*left*) and h-plane (*right*) copolar pattern (90 degrees azimuth) over elevation and frequency.

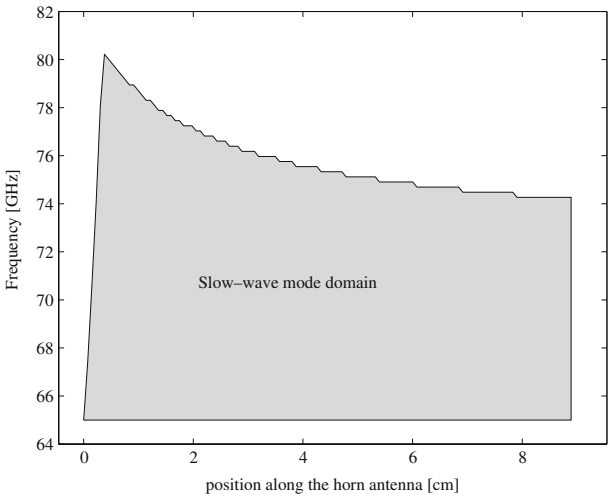

Fig. 3 Plot of the domain in the frequency- axis position space where the slow-wave modes exist.

with d being the length of one corrugation. Figure 3 shows the frequency and position along the horn where slow-wave modes exist. We also observe that both the cross-polar signal (Fig. 4) and the return loss (Fig. 9) are significantly higher for the slow-wave mode region than for the remaining pattern. Some oscillations in the sidelobe level can also be observed at the upper end of the frequency range. These variations cannot be explained to origin from slow wave modes propagating. Since the horn antenna aperture becomes electrically larger with increasing frequency diffraction at the horn aperture causes these variations.

3.2 Gaussian beam analysis

Since a corrugated horn antenna is often used as a generator of gaussian beams it is also important to analyze the properties of the corrugated horn under this aspect.

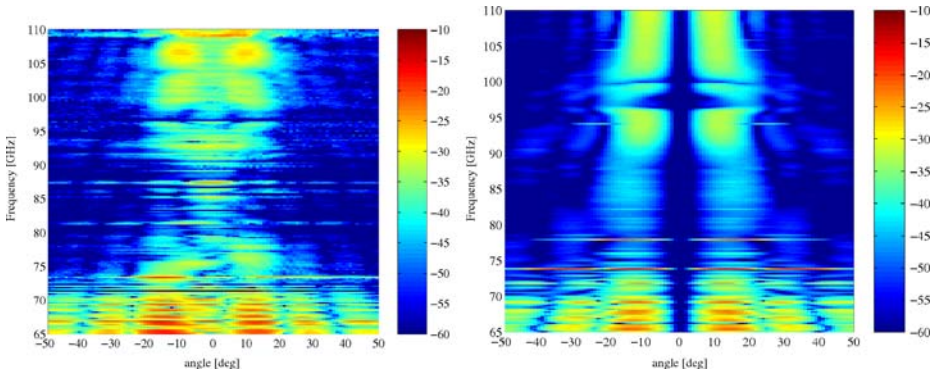

Fig. 4 Measured (*left*) and simulated (*right*) crosspolar pattern (45 degrees azimuth) over elevation and frequency.

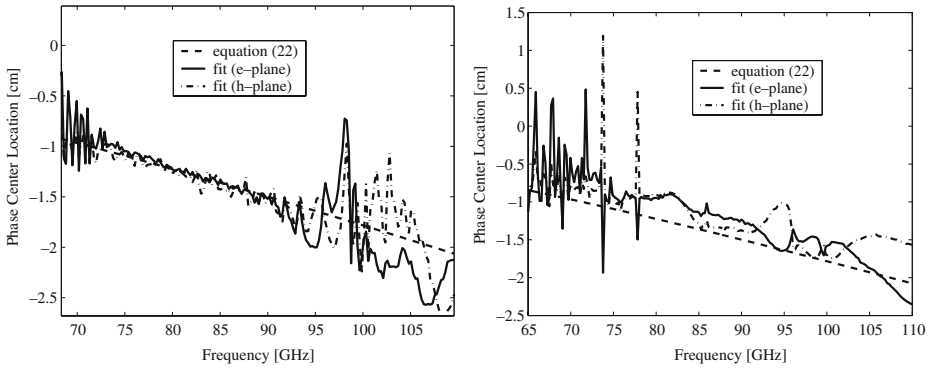

Fig. 5 Phase center with respect to the horn aperture, experimental (*left*) and model (*right*) result and approximate formula (22).

Basic work of describing the gaussian beam properties of a corrugated horn antenna has been done in [9]. The formulas developed in [9] which are

$$w_0 = \frac{0.6435a}{\sqrt{1 + \left(\frac{\pi(0.6435a)^2}{\lambda R_h}\right)^2}} \tag{21}$$

for the waist and

$$z = \frac{R_h}{1 + \left(\frac{\lambda R_h}{\pi(0.6435a)^2}\right)^2} \tag{22}$$

for the phase center with R_h being radius of curvature of the phase front at the aperture and a being the aperture radius, have been compared to data obtained by fitting a fundamental gaussian beam to both the model data and the experimental data. For the determination of the phase center we used the phase model of the method presented in [10] together with an ideal gaussian beam as an amplitude

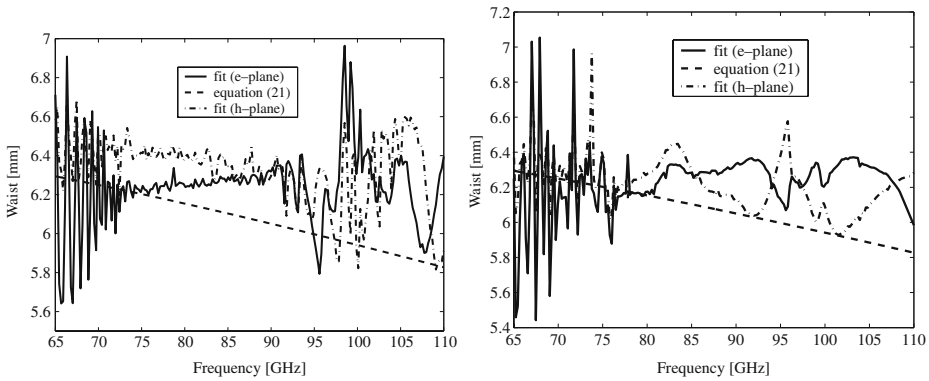

Fig. 6 Waist of the best-fit fundamental gaussian, experimental (*left*) and model (*right*) result and approximate formula (21).

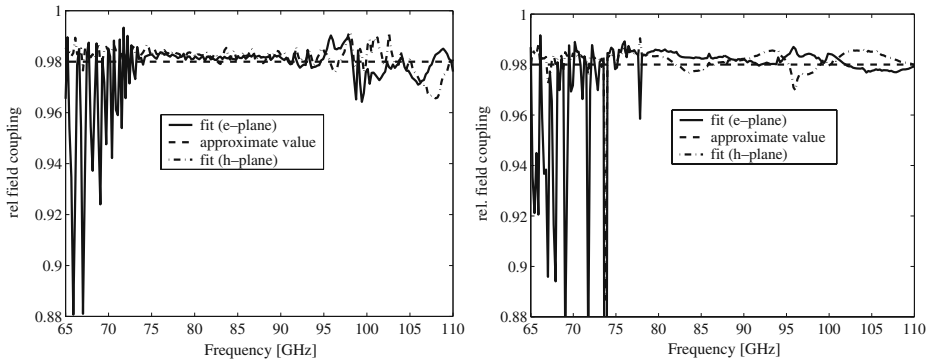

Fig. 7 Power in the best-fit fundamental gaussian, experimental (*left*) and model (*right*) result and approximate value.

pattern. The fit was done by maximizing the coupling integral between the theoretical field distribution and the measured or simulated one. This problem has been solved numerically using a Nelder-Mead optimization algorithm. The coupling into the fundamental gaussian mode has been computed using

$$C\frac{\sum E_m G^*}{\sqrt{\sum E_m E_m^*}\sqrt{\sum GG^*}} \tag{23}$$

where E_m represents the measured electric field and G the complex far-field pattern of a fundamental gaussian beam. The integration was done over a 1D cut assuming circular symmetry. Both the e-plane and the h-plane have been treated separately.

For the phase center the approximations in [9] and the retrieved parameters are in good agreement (Fig. 5). For the waist we observe an increase of the waist with frequency for the retrieved parameters and a decrease for the approximation (Fig. 6). Since the phase center position shows a similar variation for the retrieved and the approximated case we deduce that generation of higher order hybrid modes or deterioration of the surface impedance approximation mainly results in an increase

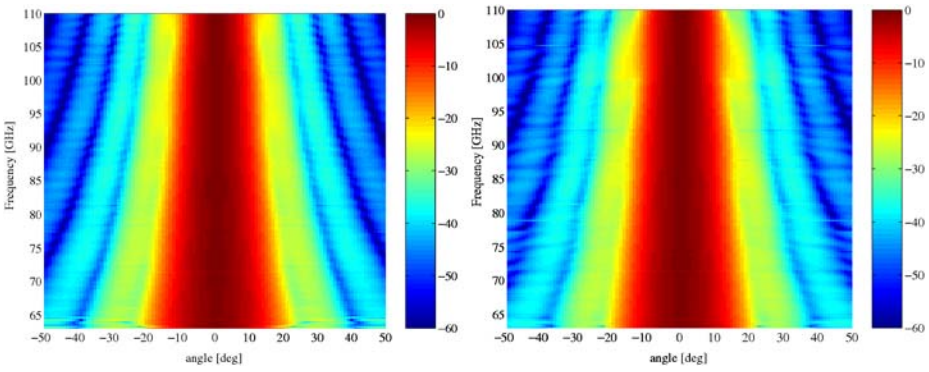

Fig. 8 Simulated e-plane (*left*) and h-plane (*right*) antenna pattern [dB] of the optimized case over elevation and frequency.

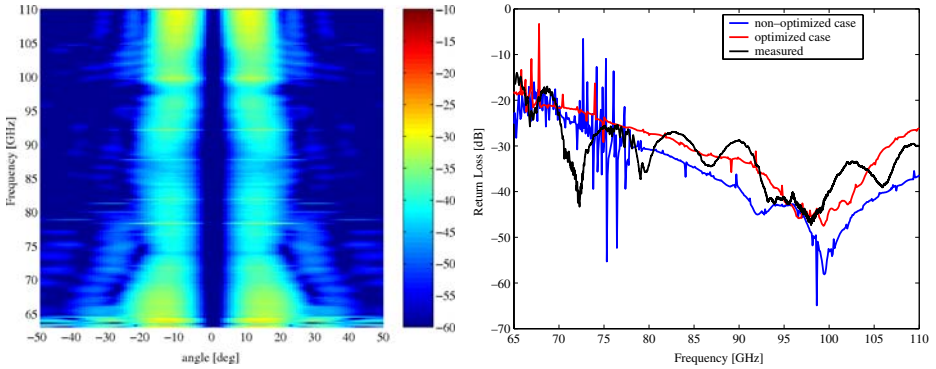

Fig. 9 *Left*: Simulated crosspolar antenna pattern [dB] of the optimized case over elevation and frequency. *Right*: Measured an simulated return losses for both the optimized and non-optimized design.

of the waist with frequency. We see also that all three parameters (Figs. 5, 6 and 7) show high oscillations for both the modelled and the experimental case in the frequency range where the slow-wave modes exist. The fluctuations in the waist wize and the phase center location visible in the upper frequency range can be explained by diffraction effects at the horn antenna aperture. Since the model results are computed using an infinite groundplane for the aperture there ar some dicrepancies between the fit results for the model data and the experimental data at the upper frequency range.

4 Suppression of the slow-wave modes

The analysis shown earlier in this paper clearly points out that presence of slow-wave modes reduces the usable bandwidth. So we must think of ways to suppress them without much complicating the horn geometry and altering the overall

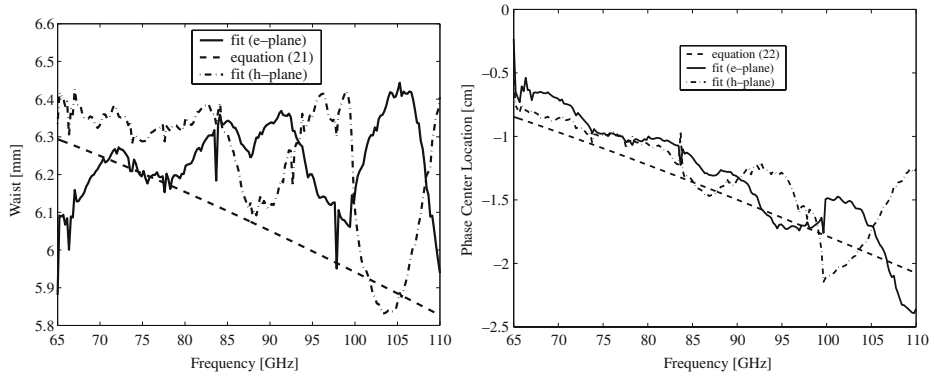

Fig. 10 *Left*: Waist of the best-fit fundamental gaussian, optimized model result and approximate formula (21). *Right*: Phase center with respect to the horn aperture, optimized model result and approximate formula (22).

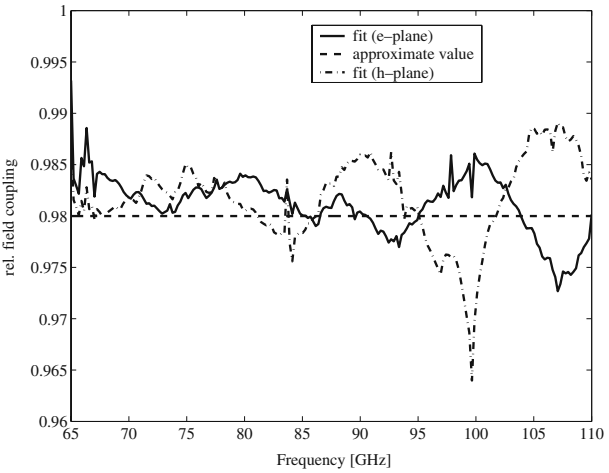

Fig. 11 Power in the best-fit fundamental gaussian, optimized model result and approximate value.

beam-pattern. The only parameter which effectively affects the presence of slow-wave modes without changing the overall beam-pattern is the corrugation size and the toothwidth ratio. Equation 20 states that increasing the corrugation width reduces the upper frequency limit of the slow-wave modes. Therefore one could simply make the corrugations larger to eliminate the problem. However, the solutions is not as simple as this. Since the entire hybrid mode theory is based on the assumption that the corrugations are infinitely small we may expect that enlargening the corrugations also reduces the overall beam quality. At this point the problem sounds contradictory: on one hand we have to make the corrugations as small as possible for the hybrid mode theory to be valid, on the other hand the corrugations should be large enough to reduce the presence of slow-wave modes.

Simulation for our specific case has shown that the corrugation width can be increased up to a factor 1.65 without significantly decreasing the pattern quality. Beyond this factor the sidelobe level at the upper end of the pattern increases rapidly. However the return loss is much affected by the corrugation width. Increasing the corrugation width immediately rises the return loss over the entire bandwidth. This can be corrected by some extent by adjusting the slotwidth to toothwidth ratio. The optimum tradeoff between suppression of slow-wave modes and low return loss has been found at a total corrugation length of 1.2mm and a tooth width to slot width ratio of 0.378. The optimized design shows a significant decrease of the spikes in the farfield pattern (Figs. 8 and 9), the return loss (Fig. 9) and all three gaussian beam parameters (Figs. 10 and 11).

5 Conclusion

The presence and impact of slow-wave modes on the antenna pattern and return loss of a corrugated W-band horn antenna has been investigated both experimentally and theoretically. It has been shown that the presence of slow-wave modes results in fast variations of the side-lobe level on both the e and h-plane pattern with frequency. Also, the slow-wave mode cause a significant increase of the maximum crosspolar

level compared with parts of the spectrum with no slow-wave modes present. The return loss curve and all gaussian beam parameters also show rapid oscillations in the slow-wave mode domain. Finally the design of the W-band horn was altered with the aim of suppressing the slow-wave modes. The investigations have shown that the slow-wave modes can be simply suppressed by increasing the corrugation width. The disadvantage is that the return loss level slightly increases over the entire band. The optimized design shows very low presence of slow-wave modes from 65 to 110 GHz.

Acknowledgements This work was supported by the Swiss National Science Foundation under Grant 200020-100167 and 200020-19908.

References

1. P. D. Potter, "A new horn antenna with suppressed sidelobes and equal bandwidths," Microwave Journal **6**, 71–78 (1963).
2. A. J. Simmons and A. F. Kay, "The scalar feed - a high-performance feed for large paraboloid reflectors," AFCRL, (1964).
3. P. Fürholz and A. Murk, "Quality Assessment of W-Band Corrugated Horn Antennas," in *Proceedings of the EuCap2007*, Edinburgh, 2007, pp. 1–6.
4. A. K. Bhattacharyya, "High-Q resonances due to surface waves and their effects in the performances of corrugated horns," IEEE Transactions on Antennas and Propagation **49**(4), 555–566 (2001).
5. *Method of Moments in Electromagnetics* (IEEE, 1968).
6. S. M. Rao, D. R. Wilton, and A. W. Glisson, "Electromagnetic scattering by surfaces of arbitrary shape," IEEE Transactions on Antennas and Propagation **41**, 409–418 (1982).
7. *Corrugated Horns for Microwave Antennas* (IEE Electromagnetic Waves Series 18, 1984).
8. A. Wexler, "Solution of waveguide discontinuities by modal analysis," IEEE Transactions on Microwave Theory and Techniques **15**(9), 508–517 (1967).
9. R. J. Wylde and D. H. Martin, "Gaussian beam-mode analysis and phase-center of corrugated feed horns," IEEE Transactions on Microwave Theory and Techniques **41**, 1691–1699 (1993).
10. P. N. Betjes, "An algorithm for automated phase center determination and its implementation," *AMTA Conference*, 2007.